



**HAL**  
open science

## Water self-diffusion in C-S-H: Effect of confinement and temperature studied by molecular dynamics

Tulio Honorio, Helena Carasek, Oswaldo Cascudo

► **To cite this version:**

Tulio Honorio, Helena Carasek, Oswaldo Cascudo. Water self-diffusion in C-S-H: Effect of confinement and temperature studied by molecular dynamics. *Cement and Concrete Research*, 2022, 155, pp.106775. 10.1016/j.cemconres.2022.106775 . hal-03614509

**HAL Id: hal-03614509**

**<https://hal.science/hal-03614509>**

Submitted on 22 Jul 2024

**HAL** is a multi-disciplinary open access archive for the deposit and dissemination of scientific research documents, whether they are published or not. The documents may come from teaching and research institutions in France or abroad, or from public or private research centers.

L'archive ouverte pluridisciplinaire **HAL**, est destinée au dépôt et à la diffusion de documents scientifiques de niveau recherche, publiés ou non, émanant des établissements d'enseignement et de recherche français ou étrangers, des laboratoires publics ou privés.



Distributed under a Creative Commons Attribution - NonCommercial 4.0 International License



Contents lists available at [ScienceDirect](https://www.sciencedirect.com)

## Cement and Concrete Research

journal homepage: [www.elsevier.com/locate/cemconres](http://www.elsevier.com/locate/cemconres)



# Water self-diffusion in C-S-H: Effect of confinement and temperature studied by molecular dynamics

Tulio Honorio<sup>a,\*</sup>, Helena Carasek<sup>b</sup>, Oswaldo Cascudo<sup>b</sup>

<sup>a</sup> Université Paris-Saclay, CentraleSupélec, ENS Paris-Saclay, CNRS, LMPS - Laboratoire de Mécanique Paris-Saclay, 91190 Gif-sur-Yvette, France

<sup>b</sup> Universidade Federal de Goiás, Escola de Engenharia Civil e Ambiental, PPG-GECON, Goiânia, Brazil

### ARTICLE INFO

#### Keywords:

Water and ion dynamics  
Molecular simulations  
Activation energy  
Diffusivity  
Micromechanics

### ABSTRACT

Despite the recent advances in the understanding of diffusion processes in C-S-H, there are still open questions regarding the pore-size dependence of diffusion and associated activation energy, and the transition from glassy to Fickian dominated dynamics. We perform molecular dynamics simulations in C-S-H with varying pore sizes (spanning interlayer and gel pore sizes) to investigate the pore size and temperature dependence of water and ion diffusion and activation energy. We quantify the finite-size artifacts from these simulations. The transition from glassy to Fickian-dominated dynamics occurs at an interlayer distance of 2.6 nm. In the Fickian regime, an expression using the self-diffusion of bulk water and a single activation energy captures the pore size and temperature dependence of the water self-diffusion in C-S-H. Finally, the anisotropic self-diffusion obtained from the molecular scale is used as input in mean-field homogenization to get gel diffusivity.

## 1. Introduction

Diffusion processes are crucial in durability problems involving cement-based materials and are also critical to applications in which concrete functions as a barrier (e.g. dams, sanitation structures, cement oil wells, nuclear waste disposal structures, and containment building in nuclear power plants). Transport phenomena in cement-based materials are a multiscale problem in which the pore phase (a multicomponent aqueous solution with varying composition [1,2]) and microporous phases (especially C-S-H) play the major role. Important advances in the understanding of diffusion processes in C-S-H has been observed in the last years especially from studies deploying atomistic simulations, which enables assessing with atomic-level detail the fundamental physical mechanisms at the origins of diffusion. However, the following questions remain unanswered (or at least, only partially answered) to date:

- (1) How diffusion of water and ions confined in C-S-H evolve with the pore size (or confinement)?
- (2) What is the role of viscosity and finite-size effects on diffusion assessed by molecular dynamics (MD) in the case of C-S-H, and what are the effects of confinement?
- (3) How does confinement affect the temperature activation of diffusion processes in C-S-H?

Regarding the question (1), diffusion is expected to decrease with confinement due the interactions of the fluid with the pore walls, and the discrete nature (granularity) of the fluid particles [3–5]. In the case of slit pores, the diffusion coefficient parallel to the pore decreases with respect to the bulk value according to the leading order  $\sigma/d$ , in which  $\sigma$  is the diameter of the fluid molecule, and  $d$  is its distance to the pore wall [4,5]. In the case of C-S-H, water in the interlayer space is reported to exhibit glassy dynamics [6]. The “glassy” behavior of ultraconfined water molecules in C-S-H was quantified (using often different nomenclature) in the review by Mishra et al. [7] according to some of the various force fields currently in use for molecular simulations of phases in cement systems. Contrary to Fickian diffusion, in which the Mean Squared Displacement (MSD)  $\langle |\mathbf{r}(t)|^2 \rangle$  scales as  $t$ , glassy dynamics is subdiffusive at sufficiently long timescales (i.e.  $\langle |\mathbf{r}(t)|^2 \rangle$  scales as  $t^\alpha$  with  $\alpha < 1$ ). The pore size in which Fickian diffusion starts to be observed in C-S-H is yet to be determined. In order to quantify the self-diffusion of confined water in C-S-H in the pore sizes corresponding to the equilibrium basal spacing (i.e. the basal spacing in which the layers effective interactions under drained conditions reaches its minimum [8–10]; this basal spacing is expected to be the most prevalent spacing in C-S-H gel structure), Qomi et al. [11] approximated the glassy dynamics by a Fickian dynamics and obtained a self-diffusion coefficient of confined water depending on the Ca/Si of C-S-H and which is only a small fraction

\* Corresponding author.

E-mail address: [tulio.honorio-de-faria@ens-paris-saclay.fr](mailto:tulio.honorio-de-faria@ens-paris-saclay.fr) (T. Honorio).

<https://doi.org/10.1016/j.cemconres.2022.106775>

Received 28 July 2021; Received in revised form 27 October 2021; Accepted 10 March 2022

Available online 19 March 2022

0008-8846/© 2022 Elsevier Ltd. All rights reserved.

of the self-diffusion coefficient of bulk water  $D^{bulk}$ ; for low Ca/Si ratio, the self-diffusion of confined water is  $0.0006D^{bulk}$  and increases as a function of the Ca/Si reaching  $0.0018D^{bulk}$  at high Ca/Si.

Various authors have investigated diffusion according to specific (slit) pore sizes in C-S-H. The first successful attempt to compare molecular modeling results with experimental observations was done by Korb et al. [12] based on the molecular dynamics simulations of a simplified C-S-H model proposed by Kalinichev et al. [13] using ClayFF. Hou and Li [14] assessed the diffusion of water, calcium counterions, and chloride ions in tobermorite nanopores of 6.5 nm thickness using MD. These authors provide profiles of self-diffusion coefficient highlighting the reduction in dynamics adjacent to the pore surface: the self-diffusion at the core retrieves bulk value and is more than three-fold the value of the self-diffusion of water near the surface. Sun et al. [15] studied the effect of confinement in water dynamics in C-S-H considering three pore sizes (0.5, 0.75, and 1 nm) and obtained similar MSD corresponding to a subdiffusive regime. Duque Redondo et al. [16] observed a reduction in water and cesium dynamics in molecular simulations of C-S-H with an 1 nm pore and a dependence of dynamics on the Ca/Si of C-S-H. Tang et al. [17] reported anisotropy in the diffusion of water confined in 6 nm thick pore in C-S-H, with in-plane diffusion roughly three-fold the out-of-plane diffusion.

Systematic and more detailed information on the self-diffusion of water confined in intermediary and larger pore sizes, and the threshold pore size from which water dynamics change from glassy to Fickian-dominated dynamics is valuable input for multiscale modeling accounting for pore size distributions in C-S-H. Furthermore, diffusion perpendicular to the pore plane is either neglected in some studies or erroneously assessed using Fickian dynamics. The dynamics perpendicular to the walls in a slit pore involves collisions with the pore walls and the effects of the confinement in fluid ordering. These phenomena lead to an overall non-Fickian dynamics which is subdiffusive at large timescales [18]. A well-suited theoretical framework to treat diffusion perpendicular to the pore plane has been proposed in the literature [19,20], but this is yet to be applied in the case of C-S-H.

Regarding question (2), finite-size effects are known to introduce artifacts in MD simulations of diffusion [21]. This artifact originates from the viscous couplings of the atoms with their periodic images, which leads to a deceleration of the dynamics [3,22]. In the case of isotropic systems, the size-independent self-diffusion coefficient  $D(\infty)$  can be computed from the diffusion coefficient  $D^{PBC}(L)$ , obtained using periodic boundary conditions (PBC) in a simulation box with length  $L$ , by [21,23,24]:

$$D(\infty) = D^{PBC} + \frac{kT\xi}{6\pi\eta L} \quad (1)$$

where  $\eta$  is the shear viscosity of the fluid, and  $\xi \approx 2.837298$  is the self-term for a cubic lattice at room temperature. Finite-size corrections for confined liquids are proposed in the literature [3] (the case of slit pore geometry, relevant to C-S-H, is detailed in Section 2.1.1). This correction has been considered in a recent study on bulk ionic solutions mimicking the pore solutions in cement systems [25]. However, the studies dealing with diffusion in C-S-H often do not take into account finite-size corrections.

Finally, concerning question (3), Qomi et al. [11] computed the energy of activation  $E_a$  of water in C-S-H with equilibrium basal spacing and observed an  $E_a$  of 11.6 kJ/mol at low Ca/Si ratios (Ca/Si = 1.2) that decreases with the Ca/Si reaching 7.7 kJ/mol at Ca/Si = 2.05. These values being lower than the value of  $E_a$  reported for bulk water ( $17.4 \pm 0.2$  kJ/mol) suggest that the activation energy is pore size-dependent. Zehtab and Tarighat [26] computed the energy of activation of ions confined in tobermorite and jennite slit pores of roughly 7 nm. Their results suggest a heterogeneous  $E_a$  of water diffusion along with the thickness of the slit pore (although this effect is not quantified in their study). Since water dynamics is expected to change significantly in the

Fickian-glassy transitions in C-S-H, repercussions in the energy of activation are also expected. Also, provided the anisotropy in diffusion, the energy of activation may show some anisotropy in confined systems. These effects are still to be studied in the case of C-S-H.

In this work, we propose to answer the three questions above using MD simulations in C-S-H systems with varying pore sizes spanning interlayer and gel pore sizes. We perform molecular dynamics simulations to compute the mean-square displacement of water and ions. The relevant finite-size corrections are applied. Liquid-Fickian and glassy regimes are identified according to the pore size. Self-diffusion coefficient and respective activation energies are computed accounting for the anisotropy. Finally, we use mean-field homogenization to upscale the anisotropic self-diffusion obtained from the molecular scale up to the gel scale.

## 2. Molecular models and methods

### 2.1. Self-diffusion coefficients under confinement from MD

Provided the layered structure of C-S-H at the molecular scale the tensor of diffusion has the form:

$$\mathbf{D} \begin{pmatrix} z \\ z \\ z \end{pmatrix} = \begin{pmatrix} D_{\parallel}(z) & 0 & 0 \\ 0 & D_{\perp}(z) & 0 \\ 0 & 0 & D_{\perp}(z) \end{pmatrix} \quad (2)$$

where parallel  $D_{\parallel}(z)$  and perpendicular  $D_{\perp}(z)$  components are inhomogeneous along  $z$  direction, and the components along  $x$  and  $y$  direction are assumed to be identical  $D_x = D_y \equiv D_{\perp}$  (which deserves to be verified under ultraconfinement, in which water molecules might exhibit anisotropic in-plane response. See Appendix A for this verification).

The components of the tensor of diffusion can be computed using (equilibrium) molecular dynamics simulations as detailed in the following.

#### 2.1.1. Diffusion parallel to the walls in a slit pore

Using Einstein formula, the parallel components of the diffusion tensor can be computed by (e.g. [27]):

$$D_{\parallel}^{EK} = \frac{1}{4} \lim_{t \rightarrow \infty} \frac{\langle [r_x(t)]^2 + [r_y(t)]^2 \rangle}{t} \quad (3)$$

where  $r_i$  ( $i = x, y$ ) are the components of the displacement vector  $\mathbf{r}(t) = \mathbf{p}(t) - \mathbf{p}(0)$ , function of the position  $\mathbf{p}$  of the particle at time  $t$ .

Fluids dynamics are known to be affected by the periodic boundary conditions (PBC) in MD simulations: atoms interact with their periodic images replicas generating viscous couplings resulting in dynamics deceleration [3,22]. Corrections for these finite-size effects are proposed in the literature for slit pore geometries [3]:

- Elongated box ( $H > L$ ):

$$D_{\parallel}(H > L, \infty) = D_{\parallel}^{PBC} - \frac{kT}{\eta} \left[ \frac{3}{40} \frac{H}{L^2} - \frac{\ln(1 + \sqrt{2})}{4\pi L} \right] \quad (4)$$

- Flat box ( $H < L$ ):

$$D_{\parallel}(H < L, \infty) \approx D_{\parallel}^{PBC} + \frac{1}{24} \frac{kT}{\eta} \frac{H}{L^2} \quad (5)$$

where  $H$  is the effective pore size, and  $L$  is the in-plane dimension of the simulation box ( $H/L$  is therefore the aspect ratio of the simulation box). Note that the finite-size corrections introduce a temperature dependency, which should not be confused with the temperature dependency quantified by Arrhenius thermal activation [28].

### 2.1.2. Diffusion perpendicular to the walls in a slit pore

The diffusion perpendicular to the wall in a slit pore involves collisions with the walls and the effects of the confinement potential  $V(z)$  (i.e. the energy profile describing the minimum free energy path [29]) resulting in an overall non-Fickian dynamics. At short timescales  $t \ll H^2/D_\perp$ , the dynamics of a single particle should be Fickian because the particle has not yet experienced any collision on the confining walls or been subjected to the restoring force from the confinement potential [30]. At larger timescales, a subdiffusive regime takes place.

The MSD along z-direction  $\langle [r_z(t)]^2 \rangle$  can be linked to diffusion coefficient  $D_\perp$  using a formalism based on Smoluchowski equation, in which the collisions and, in a simplified fashion, the confinement potential  $V(z)$  (assumed as constant) are taken into account [19]:

$$\langle [r_z(t)]^2 \rangle = \frac{H^2}{6} - \frac{16H^2}{\pi^4} \sum_{n=1(\text{odd})}^{\infty} \frac{1}{n^4} \exp \left[ -D_\perp \left( \frac{n\pi}{H} \right)^2 t \right] \quad (6)$$

Within this formalism, the diffusion model is equivalent to a free Brownian diffusion within an infinitely high square well potential [19]. In agreement with was discussed above, at times  $t = 0$ , the slope of the MSD profile is proportional to  $D_\perp$ , as in the Fickian case; then, the MSD goes asymptotically to  $H^2/6$ , as a manifestation of a subdiffusive regime [19].

Finite-size corrections have been proposed for  $D_\perp$  following the form of Eq. (1) [31]:

$$D_\perp(\infty) = D_\perp^{PBC} + \frac{kT\xi_\perp}{6\pi\eta L} \quad (7)$$

where  $\xi_\perp$  is a function of the aspect ratio  $H/L$  of the simulation box: for large aspect ratios (elongated simulation box)  $\xi_\perp \rightarrow 2.925$  and for small aspect ratios (flat box)  $\xi_\perp$  diverges as  $-(H/L)^{-2}$ .

### 2.1.3. Shear viscosity

The shear viscosity of the fluid is important to compute the finite-size correction as exposed previously. The shear viscosity can be computed using the Green-Kubo formalism with the expression [32]:

$$\eta = \frac{1}{5} \sum_{\alpha\beta} \lim_{t \rightarrow \infty} \frac{V}{kT} \int_{t=0}^{\infty} \langle p_{\alpha\beta}(t) p_{\alpha\beta}(0) \rangle dt \quad (8)$$

where  $p_{\alpha\beta}$  are three out-of-diagonal components of stress tensor  $p_{xy}$ ,  $p_{xz}$ , and  $p_{zy}$ , and the differences between the diagonal elements  $(p_{xx} - p_{yy})/2$  and  $(p_{yy} - p_{zz})/2$ . The stress auto-correlations in Eq. (8) decay fast (within a few picoseconds), which enable adopting an upper integration limit of 5 ps in order to get good estimates of the shear viscosity [33].

Contrary to diffusion, computations of the viscosity of SPC/E water are reported to be insensitive to simulation cell size [21].

## 2.2. Effective pore size

An estimate of the effective pore size  $H$  is a key element to elucidate dynamics under confinement. The determination of the exact position of the interface between the solid and the fluid is not a trivial task, especially for angstrom pores and rough surfaces (as is the case of C-S-H). Various strategies have been proposed in the literature to locate this interface:

- Gibbs dividing surface computed from density or property profiles (e.g. dielectric permittivity [34]).
- a Green-Kubo expression in terms of force and pressure cross-correlation functions [35].
- Deconvolution of water density profiles computed perpendicular to the pore plane [36].
- Expert judgement based on density profiles [37] (with a possible definition of an interphase [16]).

Here, we propose to define  $H$  from fitting the out-of-plane MSD with Eq. (7).

## 2.3. C-S-H atomistic model and force field

We adopt the atomistic C-S-H model of Kunhi et al. [38], with molecular formula  $C_{1.67}SH_n$  (in cement notation). We consider a varying water content  $n$  as a function of the basal spacing based on Grand Canonical Monte Carlo (GCMC) simulations of a previous study [39]. Fig. 1 (A) shows the water content obtained by GCMC simulations as a function of the basal spacing. The inset highlights the discrete ordering of water molecules (forming plateaus for each water layer) in small basal spacings (or angstrom pores). Fig. 1 (B) shows some of the system studied here according to the basal spacing  $d$ . The total c-length of the simulation box and indication of the effective pore size  $H$  are also shown for reference. The basal spacing of equilibrium  $d_{eq} = 13.7 \text{ \AA}$  is also indicated [39].

The interactions among atoms are modelled based on ClayFF [40] and SPC/E water model [41]. The potential energy writes:

$$U^{tot} = 4 \sum_{i \neq j, ij \text{ nonbonded}} \epsilon_{ij}^{LJ} \left[ \left( \frac{\sigma_{ij}^{LJ}}{r_{ij}} \right)^{12} - \left( \frac{\sigma_{ij}^{LJ}}{r_{ij}} \right)^6 \right] + \frac{e^2}{4\pi\epsilon_0} \sum_{i \neq j, ij \text{ nonbonded}} \frac{q_i q_j}{r_{ij}} + \sum_{ij \text{ bonded}} k_B (r_{ij} - r_0)^2 + \sum_{ijk \text{ bonded}} k_A (\theta_{ijk} - \theta_0)^2 \quad (9)$$

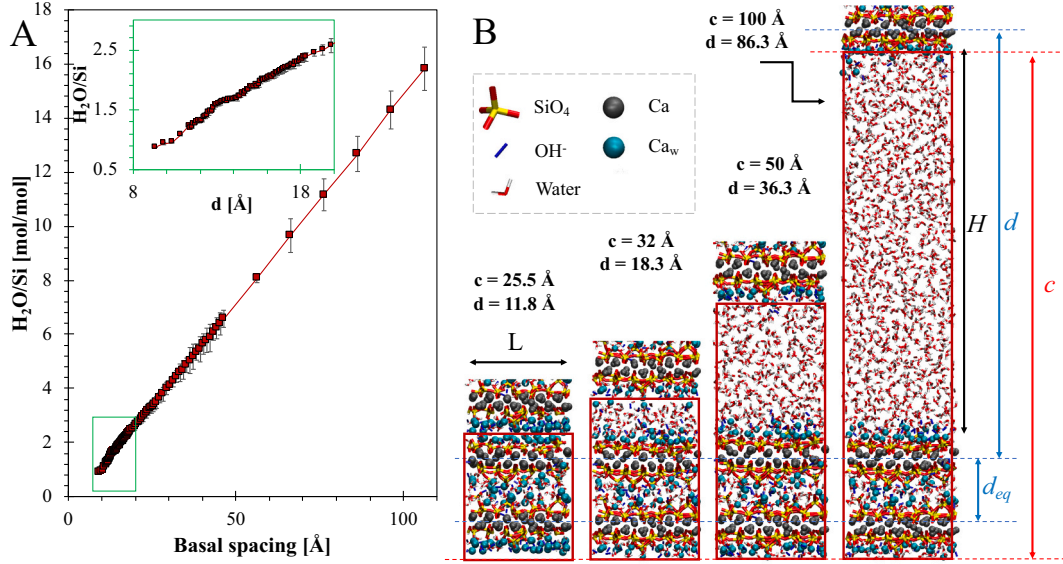
where  $r_{ij}$  is the distance between particle  $i$  and  $j$ ;  $\epsilon_{ij}^{LJ}$  and  $\sigma_{ij}^{LJ}$  are the Lennard-Jones parameters for the pair of particles  $i, j$ ;  $e$  is the elementary charge;  $\epsilon_0 = 8.85419 \times 10^{-12} \text{ F/m}$  is the dielectric permittivity of vacuum;  $q_i$  is the partial charge;  $k_B$  and  $k_A$  are the bond and angle rigidities, respectively, of the harmonic potentials;  $r_0$  and  $\theta_0$  are, respectively, the equilibrium distance and angle.

Table 1 gathers the non-bond parameters for Lennard-Jones and Coulomb potential. Lorentz-Berthelot mixing rule is adopted to compute Lennard-Jones interactions involving dissimilar elements. Table 2 gathers the parameters of the harmonic potentials for covalent bonds and angles.

## 2.4. Computational details

In all simulations, Ewald sum method with accuracy of  $10^{-5}$  is deployed to cope with long-range electrostatics; and tail corrections, for long-range Lennard-Jones interactions. A timestep of 1 fs is adopted.

The atomic configurations equilibrated at various temperatures and RH obtained from ref. [39] are first equilibrated in a 0.1 ns NVT run (using Nosé-Hoover thermostat and damping parameter of 100 time-steps). Then, the system is equilibrated during 0.1 ns in the micro-canonical ensemble (NVE). Next, in the production run, the MSDs are obtained from NVE simulations. NVE simulations are used in production since the fictitious forces associated with the thermostat (or barostat if NPT is used) may affect the dynamics [42]. After equilibration, the MSD data is collected during a 1 ns run, being recorded each 1 fs. This simulation length of 1 ns is enough to capture Fickian regime in water bulk systems. It must be noted that as a good practice very long time should be excluded from the analysis due to the increased noise sampling [42]. Twelve independent trajectories are considered for each case treated here (i.e. for each temperature and pore size). Mean and standard deviations are computed from the results of the twelve simulations.



**Fig. 1.** (A) Water content obtained by GCMC simulations from ref. [39] as a function of the basal spacing. The inset shows the plateaus associated with discrete water layering in angstrom pores. (B) Snapshots of four system studied here according to the basal spacing. For reference, the total  $c$ -length of the simulation box, the effective pore size  $H$ , and the basal spacing of equilibrium  $d_{eq} = 13.7 \text{ \AA}$  are also indicated. The  $a$ - and  $b$ -lengths are, respectively,  $22.35 \text{ \AA}$  and  $22.04 \text{ \AA}$ .

**Table 1**  
Non-bond parameters and partial charges.

Species and symbol	Partial charge [e]	$\epsilon^{IJ}$ [kJ/mol]	$\sigma^{IJ}$ [Å]
water hydrogen, H <sub>w</sub>	0.4238	–	–
water oxygen, O <sub>w</sub>	–0.8476	0.650	3.166
hydroxyl hydrogen, H <sub>H</sub>	0.4238	–	–
hydroxyl oxygen, O <sub>H</sub>	–1.4238	0.650	3.166
oxygen, O	–1.164	0.650	3.166
silicon (tetr.), Si	2.1	$7.701 \times 10^{-6}$	3.302
calcium (intra), Ca	1.05	$2.104 \times 10^{-5}$	5.567
calcium (inter), Ca <sub>w</sub>	2.00	$2.104 \times 10^{-5}$	2.872

**Table 2**  
Bond parameters (for SPC/E water and hydroxide).

	$k_B$ [kJ.mol <sup>-1</sup> .Å <sup>-2</sup> ]	$r_0$ [Å]
O <sub>w</sub> -H <sub>w</sub>	2318.500	1.0
O <sub>H</sub> -H <sub>H</sub>	2318.500	0.954
	$k_A$ [kJ.mol <sup>-1</sup> .rad <sup>-2</sup> ]	$\theta_0$ [°]
H <sub>w</sub> -O <sub>w</sub> -H <sub>w</sub>	191.50	109.47

### 3. Upscaling the diffusivity in C-S-H

#### 3.1. Mean-field homogenization of the diffusion in a micro-anisotropic system

To upscale the information from the molecular scale we adopt mean-field homogenization estimates [43]. Similar strategies have been up to upscale the thermal conductivity of C-S-H [44,45]. By mathematical analogy, the diffusion problem is akin to the thermal and electrical conductivity problem and therefore the same mathematical expressions apply [46].

The effective diffusivity of a  $N$ -phase heterogeneous material composed of anisotropic ellipsoids can be estimated using (e.g. [46]):

$$\bar{\mathbf{D}} = \sum_{p=1}^N f_p \mathbf{D}_p : \mathbf{A}_p \quad (10)$$

where  $\mathbf{D}_p$  and  $f_p$  are the diffusivity tensor (assuming a uniform diffusivity per phase) and volume fraction, respectively, of phase  $p$ ; and  $\mathbf{A}_p$  is the

localization tensor of phase  $p$ . For the case of a heterogeneous material with no phase functioning necessarily as a hosting matrix, the Self-Consistent approach can be used to estimate  $\mathbf{A}_p$  with (e.g. [46]):

$$\mathbf{A}^{SC} = \left( \mathbf{I} + \mathbf{S}_p^E : [(\bar{\mathbf{D}})^{-1} \mathbf{R} \mathbf{D}_p \mathbf{R}^T - \mathbf{I}] \right)^{-1} : \left( \sum_{r=1}^N f_r \left( \mathbf{I} + \mathbf{S}_r^E : [(\bar{\mathbf{D}})^{-1} \mathbf{R} \mathbf{D}_r \mathbf{R}^T - \mathbf{I}] \right)^{-1} \right)^{-1} \quad (11)$$

where  $\mathbf{I}$  is the (second rank) identity tensor,  $\mathbf{R}$  is the rotation matrix, and the components of the diagonal (second rank) Eshelby-like tensor  $\mathbf{S}_p^E$  of phase  $p$  (see the Appendix B for the respective formulations). Assuming that all orientations of the equiaxed particles are equally possible, the following implicit expression is obtained for the case of a 2-phase heterogeneous material composed of transverse isotropic phases (i.e.  $D_x, p = D_y, p = D_{||, p}$  and  $D_z, p = D_{\perp, p}$ ):

$$\bar{D} = \frac{\frac{7(1-\phi)D_{||,s}}{D_{||,s}+2\bar{D}} + \frac{5(1-\phi)D_{\perp,s}}{D_{\perp,s}+2\bar{D}} - \frac{7\phi D_{||,g}}{D_{||,g}+2\bar{D}} - \frac{5\phi D_{\perp,g}}{D_{\perp,g}+2\bar{D}}}{\frac{7(1-\phi)}{D_{||,s}+2\bar{D}} + \frac{5(1-\phi)}{D_{\perp,s}+2\bar{D}} - \frac{7\phi}{D_{||,g}+2\bar{D}} - \frac{5\phi}{D_{\perp,g}+2\bar{D}}} \quad (12)$$

where the subscripts <sub>s</sub> and <sub>g</sub> stand, respectively, for the solid C-S-H particle and gel porosity. An explicit solution for the real root of Eq. (12) can be obtained but is not reported here because too lengthy.

#### 3.2. Representation of the C-S-H gel microstructure

We assume that C-S-H at the gel scale is composed of two phases: C-S-H microporous particles and gel porosity. The C-S-H microporous particles are represented by transverse isotropic inclusion composed of C-S-H layers stacked according to the equilibrium basal spacing  $d_{min} = 13.7 \text{ \AA}$ . This choice is appropriate because the equilibrium basal spacing should be the most prevalent configuration in 2D-stacked systems. Evidence from experiments [47] and coarse-grained simulations [48] shows the preference of the system to exhibit stacked configurations. The gel porosity is also considered as with a transverse isotropic behavior as a function of the results of MD simulations. A characteristic pore diameter of 3 nm is adopted (e.g. [49]). Under these assumptions, Eq. (12) can be used to estimate the diffusivity and conductivity of the gel. Fig. 2 shows a simplified representation of the multiscale approach adopted in this work.

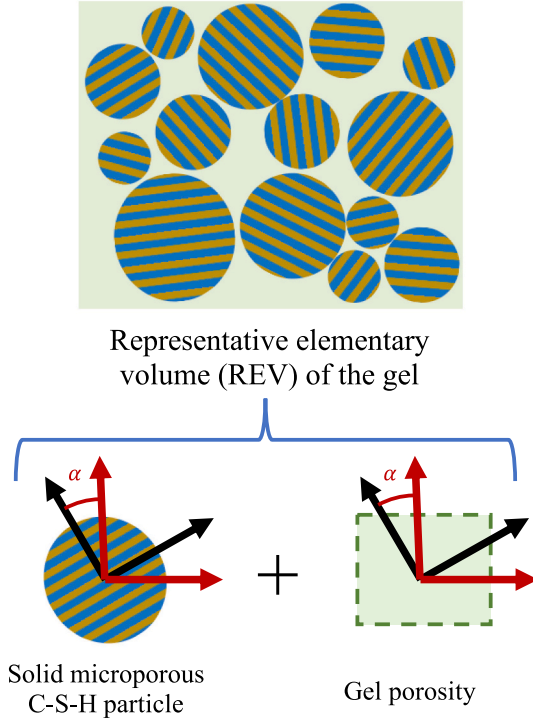


Fig. 2. Simplified representation of the gel microstructure by an assembly of transverse isotropic particles: The solid microporous C-S-H particles are represented by the spherical particles composed of stacked layers. At the bottom we depict the direction of the anisotropy (black axis) compared to a Cartesian frame (red axis). The gel porosity is the space left by the solid particles. We also adopt a transverse isotropic behavior for the gel porosity, and this behavior is also represented according to the direction of the anisotropy (black axis) compared to a Cartesian frame (red axis). (For interpretation of the references to colour in this figure legend, the reader is referred to the web version of this article.)

## 4. Results

### 4.1. Bulk water

Table 3 gathers the self-diffusion coefficient and viscosity of bulk water obtained from MD as a function of the temperature compared to experimental values. The corrected size-independent self-diffusion

Table 3

Self-diffusion coefficient and viscosity of bulk water as a function of the temperature:  $D^{PBC}$ : self-diffusion coefficient obtained from MD simulation with PBC;  $D(\infty)$ : size-independent self-diffusion coefficient obtained using Eq. (1);  $D^{Exp}$ : experimental self-diffusion of water (interpolated from the values in ref. [50]);  $\eta$ : shear viscosity of water obtained from MD simulations;  $\eta^{Exp}$  experimental shear viscosity of water (interpolated from the data in refs. [28,51]); and  $E_a$ : activation energy of diffusion.

T [K]	$D^{PBC}$ [ $10^{-9}$ m <sup>2</sup> /s]	$D(\infty)$ [ $10^{-9}$ m <sup>2</sup> /s]	$D^{Exp}$ [ $10^{-9}$ m <sup>2</sup> /s]	$\eta$ [mPa.s]	$\eta^{Exp}$ [mPa.s]
280	1.19 ± 0.27	1.42 ± 0.43	1.40	1.49 ± 0.36	1.45
290	1.60 ± 0.17	1.92 ± 0.64	1.86	1.03 ± 0.24	1.14
300	2.02 ± 0.19	2.37 ± 0.67	2.41	0.84 ± 0.23	0.86
310	2.61 ± 0.27	3.07 ± 0.47	3.02	0.76 ± 0.36	0.73
320	2.91 ± 0.23	3.43 ± 0.86	3.74	0.66 ± 0.19	0.57
$E_a$ [kJ/mol]	16.9	16.7	17.4 ± 0.2		

coefficient  $D(\infty)$  (obtained using Eq. (1)) is in better agreement with experimental values than the (uncorrected) self-diffusion coefficient obtained directly from MD simulation with PBC. The viscosity and diffusion energy of activation obtained from simulations show a good agreement with experimental values. Our results are also in agreement with previous MD studies using SPC/E water model including Smith et al. [52] ( $D = 1.62 \times 10^{-9}$  m<sup>2</sup>/s and  $\eta = 1.39$  mPa.s at 277 K;  $D = 2.68 \times 10^{-9}$  m<sup>2</sup>/s and  $\eta = 0.82$  mPa.s at 300 K) and Tazi et al. [33] ( $D = 2.97 \pm 0.05 \times 10^{-9}$  m<sup>2</sup>/s and  $\eta = 0.64 \pm 0.02$  mPa.s at 300 K).

### 4.2. Confined diffusivity

#### 4.2.1. Water

As shown in Appendix A, the MSD along (in-plane)  $x$  and  $y$ -directions are similar, confirming that the diffusivity behavior in C-S-H slit pores can be effectively approximated as in Eq. (2).

The MSD of water oxygens, hydroxide oxygen, and interlayer calcium are shown in Fig. 3 according to the parallel and perpendicular directions. The initial ballistic scaling ( $\alpha t^2$ ) is observed for all species at short timescales. Then, for water oxygens and considering the in-plane direction, Fickian diffusion ( $\text{MSD} \propto t$ ) is observed from roughly 0.1 ps for a system with  $d \geq 26.3$  Å. Sub-diffusion is observed for smaller  $d$  as well as for the other species. Similar behavior is observed for the MSD along  $z$  direction.

The perpendicular MSD is fitted with Eq. (6) in Fig. 4 having  $D_{\perp} = D_z$  and the effective pore size  $H$  as fitting parameters. The perpendicular MSD goes asymptotically to  $H^2/6$  [19], and the smaller the pore size the faster the asymptotic regime is reached. For system with basal spacing above 46.3 Å, more than 1000 ps is needed to reach the asymptotic regime. The values of  $D_z$  fitting Eq. (6) are approximately:

$$D_z = \begin{cases} \frac{1}{10} D_z^{EK} & \text{if } d \geq 46.3 \text{ \AA}, \\ \frac{1}{6} D_z^{EK} & \text{if } d < 46.3 \text{ \AA}, \end{cases} \quad (13)$$

where  $D_z^{EK} = \frac{1}{6} \lim_{t \rightarrow \infty} \frac{\langle r_z(t)^2 \rangle}{t}$ . The PBC corrections obtained for  $D_z$  using Eq. (7) are of  $0.34 \times 10^{-9}$  m<sup>2</sup>/s for elongated simulation boxes and diverges for flat boxes, being in all cases on the order or greater than the value of  $D_z$  itself. In the absence of a more adequate PBC correction for the perpendicular self-diffusion, we do not apply this correction hereafter. The fittings in Fig. 4 provide an estimation of the effective pore size  $H$  following approximately:

$$H = \begin{cases} d - 16.4 & \text{if } d \geq 18.3 \text{ \AA}, \\ d - 13.3 & \text{if } 12.3 \text{ \AA} < d < 18.3 \text{ \AA}, \\ 0.01 & \text{if } d \leq 12.3 \text{ \AA} \end{cases} \quad (14)$$

The 16.4 Å value corresponds to the sum of “thickness” of the solid layer  $\approx 12.85$  Å (measured as the distance between the center of two outmost oxygens in each surface) and the LJ diameter of an oxygen  $\approx 3.55$  Å. Using this value for basal spacings below 16.4 Å lead, of course, to a negative value of  $H$ , which motivates the use of smaller values in Eq. (14) for  $12.3 \text{ \AA} < d < 18.3 \text{ \AA}$ .

Fig. 5 shows the parallel self-diffusion coefficient of water obtained from MD simulations with and without the PBC corrections (Eqs. (4) and (5)). The effective pore size  $H$  from Eq. (14) was used in the corrections. We compare the results with the self-diffusion of bulk SPC/E water  $D_{bulk}$  and with the results from macroscopic hydrodynamics. The latter is obtained from averaging Stokes equation over the effective width of the slit pore  $H$ , so the diffusion along the wall in a slit pore with infinite lateral dimension  $L \rightarrow \infty$  is given by [3]:

$$D^{Hydr}(H) \approx D_{bulk} \left[ 1 + \frac{9}{16} \frac{\sigma}{H} \ln \left( \frac{\sigma}{2H} \right) \right] \quad (15)$$

where  $\sigma$  is the diameter of the fluid molecule. The parallel self-diffusion

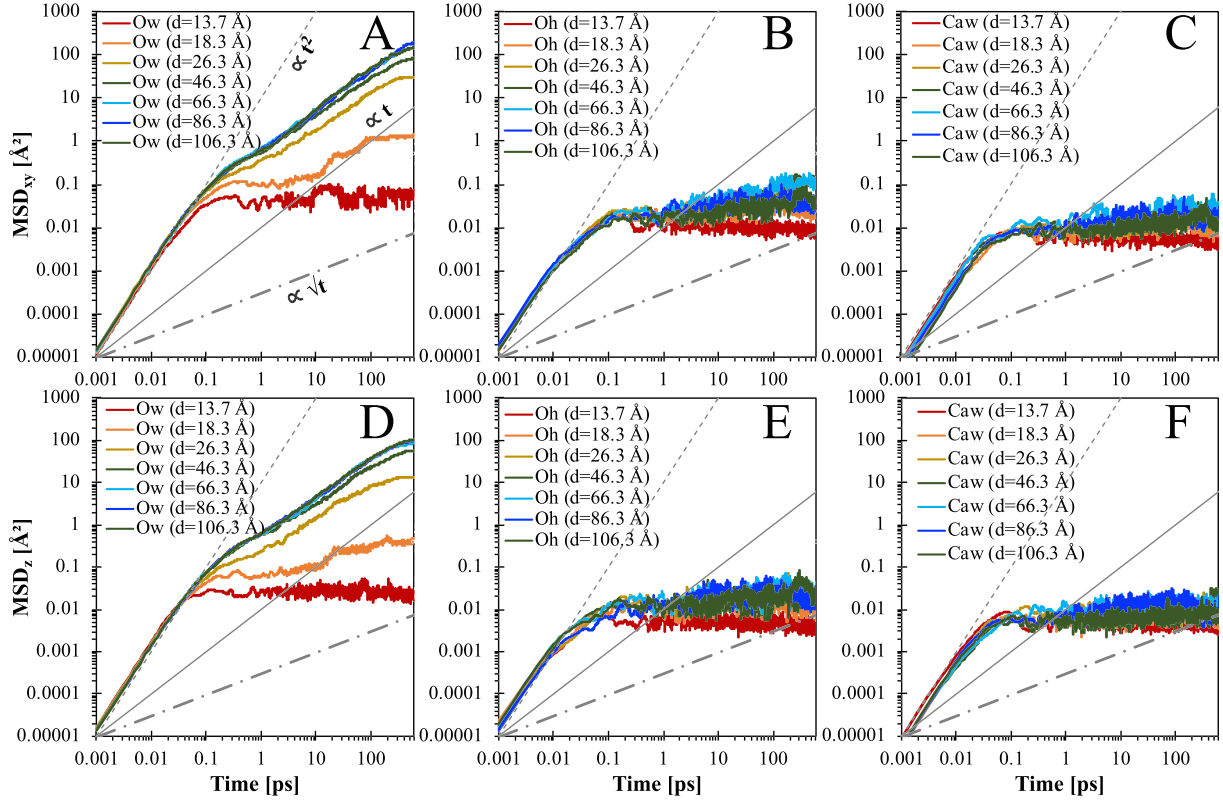


**Fig. 3.** MSD of water and ions: parallel (top) and perpendicular (bottom) components of the (A,D) water oxygen, (B,E) hydroxide oxygen, and (C,F) calcium counterion. In (A), the scalings of the MSD according to Fickian ( $MSD \propto t$ ), sub-diffusive ( $\propto t^{1/2}$ ) and super-diffusive ( $\propto t^2$ ) are shown for comparison.

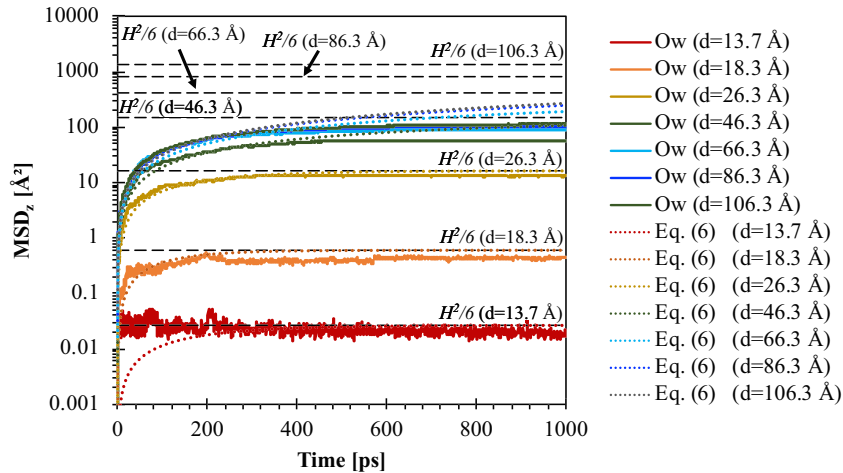


**Fig. 4.** Perpendicular component of the MSD of water (full lines) fitted with Eq. (6) (dotted lines). The dashed lines shows the  $H^2/6$  (i.e. the value to which Eq. (6) tends asymptotically) for each system considered.

coefficient of water converges to bulk value as  $d$  increases. We fit the PBC corrected values with the expression (for  $d$  in Å):

$$D_{xy}^{Fit}(d) = D_{bulk} \left( 1 - \exp \left[ -\frac{d-20}{16.7} \right] \right) \quad (16)$$

The values obtained for the self-diffusion coefficient of water are in agreement with previous studies. The parallel component of water self-diffusion for a system with the equilibrium basal spacing  $d_{min} = 13.7 \text{ \AA}$  is  $D_{xy}(d_{min}) = 0.00096D^{bulk}$ , which can be compared with previous MD simulations [11] reporting values between  $0.0006D^{bulk}$  and  $0.0018D^{bulk}$  according to the Ca/Si of the C-S-H model adopted. The volumetric

diffusivity  $D_v = Tr(\mathbf{D})/3 = (2D_{xy} + D_z)/3$  for  $d_{min} = 13.7 \text{ \AA}$  is  $1.57 \cdot 10^{-12} \text{ m}^2/\text{s}$ , which corresponds to  $0.0006D^{bulk}$ . This value can be compared with inverse analysis based on micromechanics yielding an intrinsic diffusivity of C-S-H of  $0.0004D^{bulk}$  [53].

The effect of the temperature in both parallel and perpendicular self-diffusion coefficients of water confined in C-S-H are shown in Fig. 6 (A) and (C), respectively. The simulations were performed according to five temperatures. PBC corrections are applied to the parallel self-diffusion coefficients. The profiles are fitted with an expression combining Eq. (16) with an Arrhenius term (for  $d$  in Å):

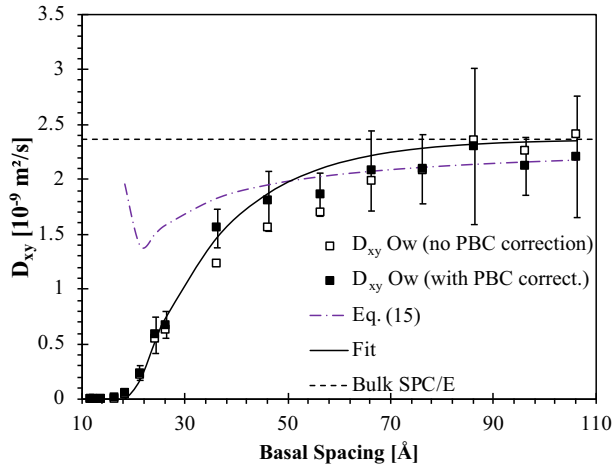


**Fig. 5.** Parallel self-diffusion coefficient of water comparison of results from MD (with and without PBC correction) and macroscopic hydrodynamics (Eq. (15)). The self-diffusion of bulk SPC/E water is shown for comparison. The PBC corrected results are fit using Eq. (16).

$$D_{xy}^{Fit}(d, T) = D_{bulk} \left( 1 - \exp \left[ -\frac{d-20}{16.7} \right] \right) \exp \left[ -\frac{E_a}{R} \left( \frac{1}{T} - \frac{1}{300} \right) \right] \quad (17)$$

where  $E_a$  is the activation energy,  $R$  is the gas constant, and  $D_{bulk}$  is the bulk value for  $T = 300$  K. Since the dynamics are reduced in the perpendicular direction, for  $D_z$  using  $D_{bulk}/14$  as the asymptotic value leads to better fittings.

The activation energy can be computed from these results as shown in Fig. 7. Different from the diffusion coefficient, no significant

anisotropy is observed in the activation energy.

We fit the activation energy profiles with the expression (for  $d$  in Å):

$$E_a(d) = -A_1(1 - \exp[-A_2(d - A_3)])^2 + A_4 \quad (18)$$

where the fitting parameter are  $(A_1, A_2, A_3, A_4) = (4.18 \text{ kJ/mol}, 0.054 \text{ 1/Å}, 30.64 \text{ Å}, 22.11 \text{ kJ/mol})$  for the parallel component, and  $(A_1, A_2, A_3, A_4) = (7.01 \text{ kJ/mol}, 0.061 \text{ 1/Å}, 27.00 \text{ Å}, 22.40 \text{ kJ/mol})$  for the perpendicular component. The activation energy exhibits a non-monotonous dependence on the pore size with a maximum at  $d \approx 28 \text{ Å}$ . This value in which the peak appears is close to the one observed for the dynamic crossover observed in Figs. 6 (B) and (D). A pronounced reduction in the dynamics along the perpendicular direction is observed. Log-Log plots Figs. 6 (B) and (D) show that two regimes can be observed with  $D_{xy}$  and  $D_z$  scaling as  $\propto d^\beta$  with  $\beta = 12 - 13$  for  $d < \approx 26 \text{ Å}$ , and  $\beta = 0.6 - 0.7$  for  $d > \approx 26 \text{ Å}$  with a small dependence of the system temperature. A previous study [39] shows that for basal spacings  $d > \approx 26 \text{ Å}$ , the radial distribution functions (RDF) of confined water are very similar to the one of bulk water. For smaller basal spaces, though, a peakier RDF is observed which indicates a significant change in water structure. Peakier RDF and slow dynamics [54] can be related to a transition from a liquid to a glassy state.

#### 4.2.2. Hydroxide and calcium ions

The estimation of expressions describing the evolution of self-diffusion coefficients of ions as a function of the basal spacing is much more challenging because of the relatively low values of self-diffusion coefficients and the relatively high standard deviation obtained from simulations. One of the reasons that make self-diffusion coefficients of ions low is the existence of hydration shells and contact ion pairs (CIP) [25,55]. Caw-OH groups form clusters that remain stable in the time-scale of the MD simulations. Fig. 8 shows the self-diffusion coefficients of

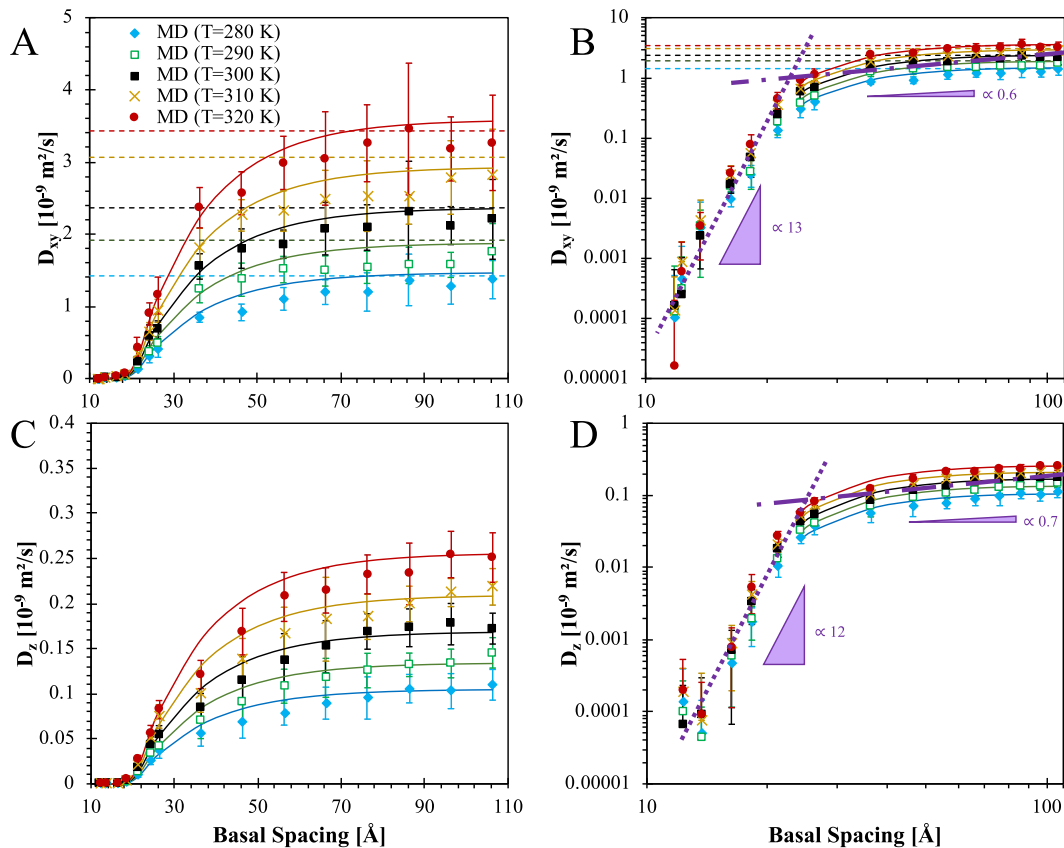


**Fig. 6.** Self-diffusion coefficient of water as a function of the basal spacing for various temperatures: (A) parallel and (C) perpendicular components; (B) and (D) respective Log-Log plots showing a dynamic crossover near  $d \approx 26 \text{ Å}$ . Full lines in (A) and (B) corresponds to fitting with Eq. (17).

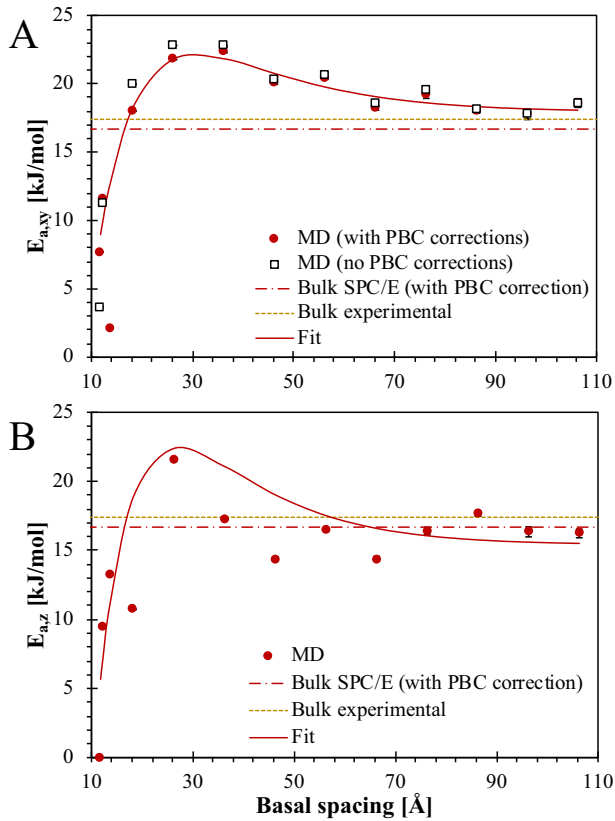


Fig. 7. Activation energy according to the: (A) parallel and (B) perpendicular self-diffusion coefficients.

hydroxide oxygen and calcium counterion from MD for various temperatures. The calcium and hydroxide diffusion is drastically reduced under confinement in C-S-H when compared to the other values in the literature. For infinitely dilute concentrations, calcium and hydroxide self-diffusion coefficients are  $0.792 \times 10^{-9} \text{ m}^2/\text{s}$  and  $5.273 \times 10^{-9} \text{ m}^2/\text{s}$ , respectively [56]. A study in mesoporous material observed a reduction in the self-diffusion of calcium confined in a slit pore [57] but less than three orders of magnitude as observed here. Simulation in bulk systems also exhibits a reduction in ions dynamics and the dielectric properties due to CIP and simple and double solvated ion pairs [25,55]. The difference can be explained due to the higher amount of CIP and hindered dynamics due to surface ion adsorption in the case of C-S-H.

Here, we adopt a similar strategy of fitting MD results with an expression like Eq. (17) but using  $D_{ion}$  as a fitting parameter. We obtain (for  $d$  in Å):

$$D_{xy}^{Fu}(d, T) = D_{ion} \left( 1 - \exp \left[ -\frac{d-20}{2} \right] \right) \exp \left[ -\frac{E_a}{R} \left( \frac{1}{T} - \frac{1}{300} \right) \right] \quad (19)$$

with  $D_{ion}=0.0015 \times 10^{-9} \text{ m}^2/\text{s}$  for Oh and  $D_{ion}=0.0003 \times 10^{-9} \text{ m}^2/\text{s}$  for Caw. The values of  $E_a=16.7 \text{ kJ/mol}$  obtained for bulk water fit well the curves for both ions. This result is in agreement with MD simulation in other layered materials in which the activation energy of confined ions was similar to water's [28].

A reactive process of proton transfer in the local aqueous environment of hydroxide ions, called Grotthuss mechanism (brought to our attention by one of the reviewers of this work), is recognized to contribute up to 50% to the diffusional mobility of hydroxide ions [58,59]. Analysis based on non-reactive force field (as is the case of ClayFF adopted here), cannot properly account for such reactive contributions to the hydroxide ions dynamics. However, several semi-empirical approaches to take this mechanism into account in the

framework of classical MD are proposed in the literature [60–62] and might be the focus of future research.

#### 4.3. Upscaling the diffusivity

To upscale the information from the molecular scale we use Eq. (12) according to the representation of the C-S-H gel structure proposed in Section 3.2. Fig. 9 shows the effective diffusivity of the C-S-H gel as a function of the gel porosity. The values at packing densities of 0.64 and 0.74, associated with low and high density C-S-H, respectively, are  $0.029 \pm 0.01 \times 10^{-9} \text{ m}^2/\text{s}$  ( $0.012D_{bulk}$ ) and  $0.0081 \pm 0.004 \times 10^{-9} \text{ m}^2/\text{s}$  ( $0.0034D_{bulk}$ ), respectively. We use the standard deviations for the diffusivities obtained from MD simulations to defined the upper and lower variability limits for our estimates. These values can be compared with the experimental data from the literature associated with gel pores or surface adsorbed water. Quasielastic neutron scattering spectroscopy experiments on C-S-H gels [63] obtained a self-diffusion coefficient for in the range 0.02–0.05  $D_{bulk}$ . Incoherent Elastic Neutron Scattering yielded 0.017  $D_{bulk}$  [64], and Proton Field Cycling Relaxometry experiments yielded 0.03  $D_{bulk}$  [12]. Our results are therefore in agreement with the available experimental evidence at the gel scale.

## 5. Conclusion

Molecular dynamics simulations were performed using realistic C-S-H models with varying pore sizes spanning interlayer and gel pore sizes in order to unveil the pore size dependence of water and ion diffusion and associated activation energy. The main conclusions that can be drawn from this work are:

- *Water and ion dynamics show a marked dependence on the C-S-H pore size.* The dynamics changes from glassy-dominated to Fickian-dominated for basal spacing above 2.6 nm. In the Fickian regime, a simple expression (Eq. (17)) using the self-diffusion of bulk water and constant activation energy captures the pore size and temperature dependence of the self-diffusion coefficient of water confined in C-S-H.
- *Diffusion activation energy exhibits a marked pore-size dependence especially under glassy dynamics regime.* The activation energy evolves non-monotonously with the pore size, reaching a maximum near the transition from glassy to Fickian-dominated dynamics. No significant anisotropy is observed for the activation energy despite the difference regarding the geometrical constraints for parallel and perpendicular dynamics.
- *Finite-size corrections are significant for small simulation boxes in C-S-H and bulk system simulations.* Periodic boundary conditions introduce artifacts in the dynamics assessed by molecular dynamics. We have adopted the relevant correction to water diffusivity and observed differences on the order of a  $0.1 - 1.0 \times 10^{-9} \text{ m}^2/\text{s}$ .
- *Mean-field homogenization allows upscaling information from the molecular scale, properly accounting for the anisotropy in the dynamics, to get gel effective diffusivity.* At the molecular scale, the diffusion parallel to the pore walls is one order of magnitude larger than the diffusion perpendicular to the pore walls. This anisotropy was accounted for in the homogenization approach. The results obtained agree with the available experimental evidence.

Perspectives of this work include considering ions relevant for durability (chloride, carbonates, sulfates, etc) or for concrete when it is used as a safety barrier (for instance, to contain radionuclides). Additionally, the effects of unsaturated conditions are also an important issue [49] yet to be addressed.

#### CRedit authorship contribution statement

**Tulio Honorio:** Conceptualization, Methodology, Investigation,

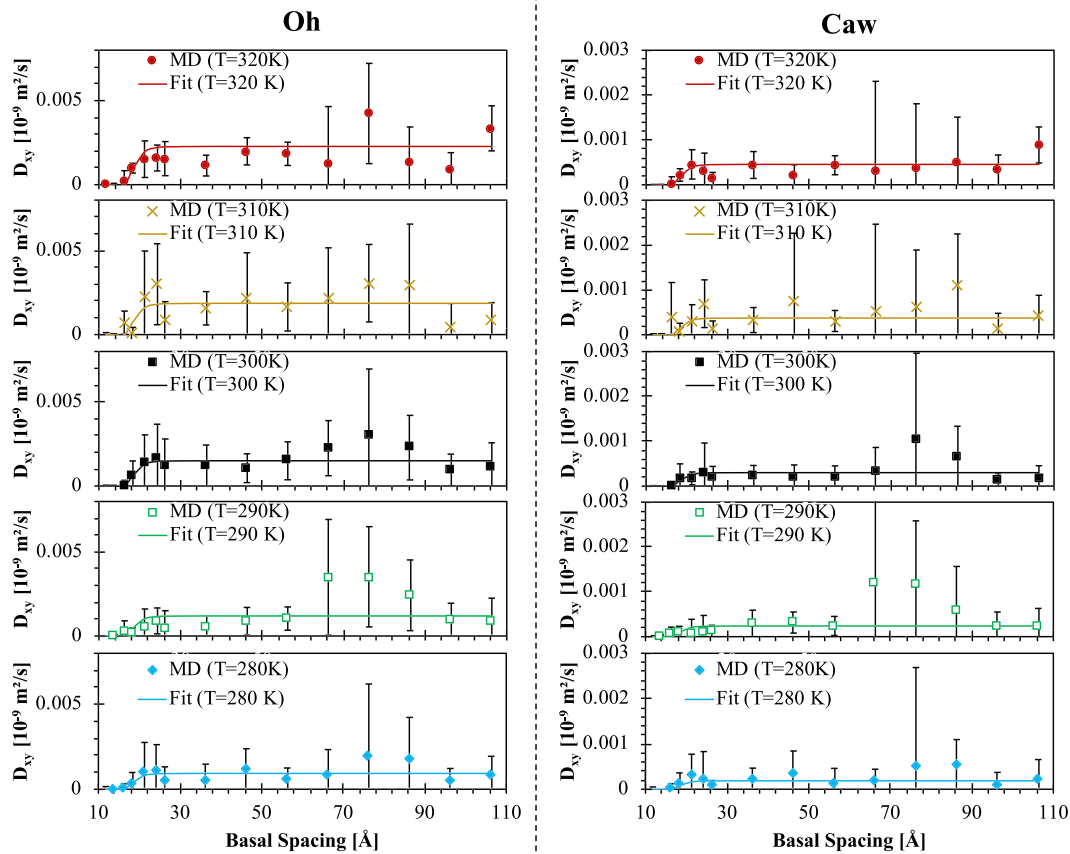


Fig. 8. Parallel component of the self-diffusion of hydroxide oxygen (at left) and calcium counterion (at right).

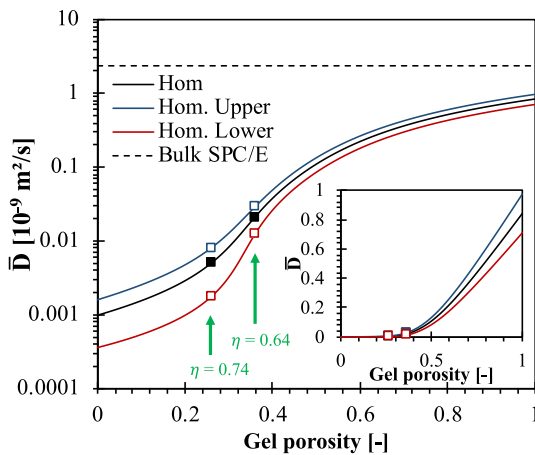


Fig. 9. Effective diffusivity of the C-S-H gel as a function of the gel porosity. Upper and lower estimates are computed as a function of the standard deviations for the diffusivities obtained from MD simulations. The values at packing densities of 0.64 and 0.74 are depicted by the squares. The inset shows the same graphic with linear scales highlighting the percolation threshold effect expected from self-consistent scheme.

Formal analysis, Writing – original draft, Validation. **Helena Carasek:**

Conceptualization, Methodology, Writing – review & editing. **Oswaldo Cascudo:** Conceptualization, Methodology, Writing – review & editing, Funding acquisition.

**Declaration of competing interest**

The authors Tullio Honorio, Helena Carasek and Oswaldo Cascudo of the manuscript “Water selfdiffusion in C-S-H: effect of confinement and temperature studied by molecular dynamics” submitted to Cement and Concrete Research declare no conflict of interest.

**Acknowledgements**

We would like to thank the company Eletronbras Furnas and the agency ANEEL - Agência Nacional de Energia Elétrica, from Brazil, for their financial support. O. Cascudo also thanks CNPq - Conselho Nacional de Desenvolvimento Científico e Tecnológico, from Brazil, which provided a research grant.

## Appendix A. In-plane diffusion

We compare the MSD along with the two orthogonal in-plane directions  $x$  and  $y$  in Fig. 10 for two basal systems associated with interlayer spaces of Angstrom size. Even under this ultraconfinement the dynamics along both in-plane directions are similar. This observation validates the strategy to compute in-plane diffusion  $D_{\parallel} = (D_x + D_y)/2 \approx D_x \approx D_y$  used in this study.

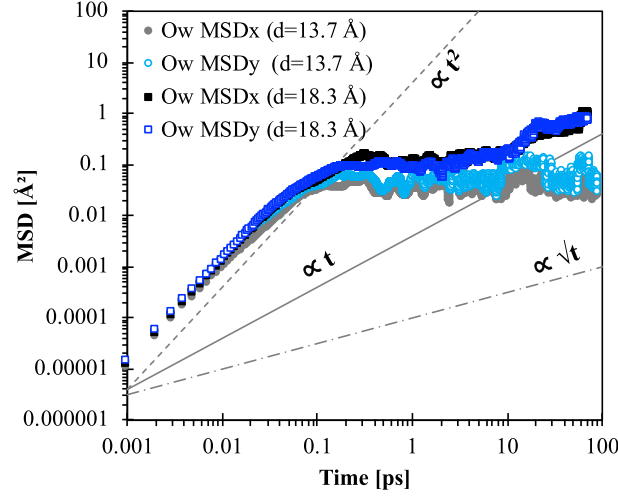


Fig. 10. MSD along  $x$ - and  $y$ -directions. The scalings of the MSD according to Fickian ( $\text{MSD} \propto t$ ), sub-diffusive ( $\propto t^{1/2}$ ) and super-diffusive ( $\propto t^2$ ) are shown for comparison.

## Appendix B. Homogenization of the diffusivity

The rotation matrix  $\mathbf{R}$  is obtained from the product:

$$\mathbf{R} = \mathbf{R}_x(\alpha)\mathbf{R}_y(\beta)\mathbf{R}_z(\gamma) \quad (20)$$

where  $\alpha$ ,  $\beta$  and  $\gamma$  are the Euler angles and the elemental rotations about  $x$ -,  $y$ - and  $z$ -axes are respectively given by:

$$\mathbf{R}_x(\alpha) = \begin{pmatrix} 1 & 0 & 0 \\ 0 & \cos\alpha & -\sin\alpha \\ 0 & \sin\alpha & \cos\alpha \end{pmatrix}$$

$$\mathbf{R}_y(\alpha) = \begin{pmatrix} \cos\alpha & 0 & \sin\alpha \\ 0 & 1 & 0 \\ -\sin\alpha & 0 & \cos\alpha \end{pmatrix}$$

$$\mathbf{R}_z(\alpha) = \begin{pmatrix} \cos\alpha & -\sin\alpha & 0 \\ \sin\alpha & \cos\alpha & 0 \\ 0 & 0 & 1 \end{pmatrix}$$

To account for the orientation for the anisotropic particles, the following operator  $\langle \cdot \rangle_R$  is applied over the localization tensor  $A_p(\alpha, \beta, \gamma)$  (e.g. [43]):

$$\langle A_p(\alpha, \beta, \gamma) \rangle_R = \frac{1}{8\pi^2} \int_0^{2\pi} \int_0^\pi \int_0^{2\pi} A_p(\alpha, \beta, \gamma) \rho(\alpha, \beta, \gamma) \sin(\beta) d\alpha d\beta d\gamma \quad (21)$$

where  $\rho(\alpha, \beta, \gamma)$  is the probability density function associated with the orientation given by the Euler angles. In the case of all orientation being equiprobable,  $\rho(\alpha, \beta, \gamma)$  is a uniform distribution.

The components of the diagonal (second rank) Eshelby-like tensor of phase  $p$  are given by [43]:

$$\mathbf{S}_p^E = \frac{a_1 a_2 a_3}{2} \int_0^\infty \frac{1}{(a_i^2 + s) \sqrt{\prod_{i=1}^3 (a_i^2 + s)}} ds \quad (22)$$

where  $a_1$ ,  $a_2$  and  $a_3$  are the semi-axes of the ellipsoid. in the case of a sphere,  $S_{11}^E = S_{22}^E = S_{33}^E = 1/3$ . A simple expression can also be found for elliptic cylinders, penny shapes, oblate and prolate spheroids [43].

For the case of a 2-phase heterogeneous material composed of equiaxed inclusions with one of the phases exhibiting isotropic diffusivity  $D_{\parallel}$  and the other phase diffusivity being describe by an transverse isotropic tensor  $\mathbf{D}_s(D_{\parallel}, D_{\perp})$  (as in Eq. (2)), Eq. (10) reduces to the implicit expression:

$$\bar{D} = \frac{\frac{7(1-\phi)D_{l,s}}{D_{l,s}+2\bar{D}} + \frac{5(1-\phi)D_{\perp,s}}{D_{\perp,s}+2\bar{D}} - \frac{12\phi D_l}{D_l+2\bar{D}}}{\frac{7(1-\phi)}{D_{l,s}+2\bar{D}} + \frac{5(1-\phi)}{D_{\perp,s}+2\bar{D}} - \frac{12\phi}{D_l+2\bar{D}}} \quad (23)$$

where  $\phi$  is the volume fraction of the phase exhibiting isotropic diffusivity.

For  $D_{||} = D_{\perp} = D_s$ , Eq. (12) reduces to explicit equation of the self-consistent scheme for a 2-phase micro- and macro-isotropic heterogeneous materials [65]:

$$\bar{D} = \frac{1}{4} \left( S_{SC} + \sqrt{S_{SC}^2 + 8D_l D_s} \right) \quad (24)$$

with  $S_{SC} = ((3\phi - 1)D_l + (2 - 3\phi)D_s)$ .

## References

- [1] A. Vollpracht, B. Lothenbach, R. Snellings, J. Haufe, The pore solution of blended cements: a review, *Mater. Struct.* 49 (8) (2016) 3341–3367.
- [2] O. Cascudo, P. Pires, H. Carasek, A. de Castro, A. Lopes, Evaluation of the pore solution of concretes with mineral additions subjected to 14 years of natural carbonation, *Cem. Concr. Compos.* 103858 (2020).
- [3] P. Simonnin, B. Noetinger, C. Nieto-Draghi, V. Marry, B. Rotenberg, Diffusion under confinement: hydrodynamic finite-size effects in simulation, *J. Chem. Theory Comput.* 13 (6) (2017) 2881–2889.
- [4] J.W. Swan, J.F. Brady, Particle motion between parallel walls: hydrodynamics and simulation, *Phys. Fluids* 22 (10) (2010), 103301.
- [5] J.R. Blake, A.T. Chwang, Fundamental singularities of viscous flow: part I: the image systems in the vicinity of a stationary no-slip boundary, *J. Eng. Math.* 8 (1) (1974) 23–29.
- [6] M. Youssef, R.J.-M. Pellenq, B. Yildiz, Glassy nature of water in an ultraconfining disordered material: the case of calcium-silicate-hydrate, *J. Am. Chem. Soc.* 133 (8) (2011) 2499–2510.
- [7] R. Mishra A. Kunhi D. Geissbühler H. Manzano T. Jamil R. Shahsavari A. G. Kalinichev S. Galmardini L. Tao H. Heinz R. Pellenq A. van Duin S. C. Parker R. Flatt P. Bowen, cemff: a force field database for cementitious materials including validations, applications and opportunities, *Cem. Concr. Res.* doi:10.1016/j.cemconres.2017.09.003.
- [8] P.A. Bonnaud, C. Labbez, R. Miura, A. Suzuki, N. Miyamoto, N. Hatakeyama, A. Miyamoto, K.J.V. Vliet, Interaction grand potential between calcium-silicate-hydrate nanoparticles at the molecular level, *Nanoscale* 8 (7) (2016) 4160–4172.
- [9] T. Honorio, Monte Carlo molecular modeling of temperature and pressure effects on the interactions between crystalline calcium silicate hydrate layers, *Langmuir* 35 (11) (2019) 3907–3916.
- [10] S. Masoumi, H. Valipour, M.J. Abdolhosseini Qomi, Intermolecular forces between nanolayers of crystalline calcium-silicate-hydrates in aqueous medium, *J. Phys. Chem. C* 121 (10) (2017) 5565–5572.
- [11] M.J.A. Qomi, M. Bauchy, F.-J. Ulm, R.J.-M. Pellenq, Anomalous composition-dependent dynamics of nanoconfined water in the interlayer of disordered calcium-silicates, *J. Chem. Phys.* 140 (5) (2014), 054515.
- [12] J.P. Korb, L. Monteilhet, P.J. McDonald, J. Mitchell, Microstructure and texture of hydrated cement-based materials: a proton field cycling relaxometry approach, *Cem. Concr. Res.* 37 (3) (2007) 295–302.
- [13] A.G. Kalinichev, J. Wang, R.J. Kirkpatrick, Molecular dynamics modeling of the structure, dynamics and energetics of mineral-water interfaces: application to cement materials, *Cem. Concr. Res.* 37 (3) (2007) 337–347, <https://doi.org/10.1016/j.cemconres.2006.07.004>. <https://www.sciencedirect.com/science/article/pii/S008884606001906>.
- [14] D. Hou, Z. Li, Molecular dynamics study of water and ions transported during the nanopore calcium silicate phase: case study of jennite, *J. Mater. Civ. Eng.* 26 (5) (2014) 930–940.
- [15] J. Sun, W. Zhang, J. Zhang, D. Hou, Molecular dynamics study the structure, bonding, dynamic and mechanical properties of calcium silicate hydrate with ultra-confined water: effects of nanopore size, *Constr. Build. Mater.* 280 (2021), 122477.
- [16] E. Duque-Redondo, K. Yamada, H. Manzano, Cs retention and diffusion in C-S-H at different Ca/Si ratio, *Cem. Concr. Res.* 140 (2021), 106294.
- [17] S. Tang, H. A. J. Chen, W. Yu, P. Yu, E. Chen, H. Deng, Z. He, The interactions between water molecules and C-S-H surfaces in loads-induced nanopores: a molecular dynamics study, *Appl. Surf. Sci.* 496 (2019), 143744.
- [18] R. Metzler, J.-H. Jeon, A.G. Cherstvy, E. Barkai, Anomalous diffusion models and their properties: non-stationarity, non-ergodicity, and ageing at the centenary of single particle tracking, *Phys. Chem. Chem. Phys.* 16 (44) (2014) 24128–24164.
- [19] A. Kusumi, Y. Sako, M. Yamamoto, Confined lateral diffusion of membrane receptors as studied by single particle tracking (nanovid microscopy). Effects of calcium-induced differentiation in cultured epithelial cells, *Biophys. J.* 65 (5) (1993) 2021–2040.
- [20] P. Liu, E. Harder, B.J. Berne, On the calculation of diffusion coefficients in confined fluids and interfaces with an application to the liquid-vapor interface of water, *J. Phys. Chem. B* 108 (21) (2004) 6595–6602.
- [21] I.-C. Yeh, G. Hummer, Diffusion and electrophoretic mobility of single-stranded RNA from molecular dynamics simulations, *Biophys. J.* 86 (2) (2004) 681–689.
- [22] R.M. Tinnacher, M. Holmboe, C. Tournassat, I.C. Bourg, J.A. Davis, Ion adsorption and diffusion in smectite: molecular, pore, and continuum scale views, *Geochim. Cosmochim. Acta* 177 (2016) 130–149.
- [23] R.E. Zeebe, On the molecular diffusion coefficients of dissolved CO<sub>2</sub>, HCO<sub>3</sub><sup>-</sup>, and CO<sub>3</sub><sup>2-</sup> and their dependence on isotopic mass, *Geochim. Cosmochim. Acta* 75 (9) (2011) 2483–2498.
- [24] A.J. Asta, M. Levesque, R. Vuilleumier, B. Rotenberg, Transient hydrodynamic finite-size effects in simulations under periodic boundary conditions, *Phys. Rev. E* 95 (6) (2017), 061301.
- [25] T. Honorio, F. Benboudjema, T. Bore, M. Ferhat, E. Vourc'h, The pore solution of cement-based materials: structure and dynamics of water and ions from molecular simulations, *Phys. Chem. Chem. Phys.* 21 (2019) 11111–11121.
- [26] B. Zehtab, A. Tarighat, Molecular dynamics simulation to assess the effect of temperature on diffusion coefficients of different ions and water molecules in C-S-H, *Mech. Time-Depend. Mater.* 22 (4) (2018) 483–497.
- [27] J.P. Boon, S. Yip, *Molecular Hydrodynamics*, Courier Corporation, 1991.
- [28] M. Holmboe, I.C. Bourg, Molecular dynamics simulations of water and sodium diffusion in smectite interlayer nanopores as a function of pore size and temperature, *J. Phys. Chem. C* 118 (2) (2014) 1001–1013.
- [29] B. Rotenberg, V. Marry, R. Vuilleumier, N. Malikova, C. Simon, P. Turq, Water and ions in clays: unraveling the interlayer/micropore exchange using molecular dynamics, *Geochim. Cosmochim. Acta* 71 (21) (2007) 5089–5101.
- [30] S. Burov, R. Metzler, E. Barkai, Aging and nonergodicity beyond the khinchin theorem, *Proc. Natl. Acad. Sci.* 107 (30) (2010) 13228–13233.
- [31] A. Botan, V. Marry, B. Rotenberg, Diffusion in bulk liquids: finite-size effects in anisotropic systems, *Mol. Phys.* 113 (17–18) (2015) 2674–2679.
- [32] J.S. Medina, R. Prosimi, P. Villarreal, G. Delgado-Barrio, G. Winter, B. González, J. V. Alemán, C. Collado, Molecular dynamics simulations of rigid and flexible water models: temperature dependence of viscosity, *Chem. Phys.* 388 (1) (2011) 9–18.
- [33] S. Tazi, A. Boğan, M. Salanne, V. Marry, P. Turq, B. Rotenberg, Diffusion coefficient and shear viscosity of rigid water models, *J. Phys. Condens. Matter* 24 (2012), 284117.
- [34] D. J. Bonhuis S. Gekle R. R. Netz, Dielectric profile of interfacial water and its effect on double-layer capacitance, *Phys. Rev. Lett.* 107 (16).
- [35] L. Bocquet, J.-L. Barrat, Hydrodynamic boundary conditions, correlation functions, and kubo relations for confined fluids, *Phys. Rev. E* 49 (4) (1994) 3079–3092.
- [36] P.A. Bonnaud, H. Manzano, R. Miura, A. Suzuki, N. Miyamoto, N. Hatakeyama, A. Miyamoto, Temperature dependence of nanoconfined water properties: application to cementitious materials, *J. Phys. Chem. C* 120 (21) (2016) 11465–11480, <https://doi.org/10.1021/acs.jpcc.6b00944>.
- [37] A. Botan, B. Rotenberg, V. Marry, P. Turq, B. Noetinger, Hydrodynamics in clay nanopores, *J. Phys. Chem. C* 115 (32) (2011) 16109–16115.
- [38] A. Kunhi Mohamed, S.C. Parker, P. Bowen, S. Galmardini, An atomistic building block description of C-S-H - towards a realistic C-S-H model, *Cem. Concr. Res.* 107 (2018) 221–235.
- [39] T. Honorio, F. Masara, F. Benboudjema, Heat capacity, isothermal compressibility, isosteric heat of adsorption and thermal expansion of water confined in C-S-H, *Cement* (2021), 100015, <https://doi.org/10.1016/j.cement.2021.100015>. <https://www.sciencedirect.com/science/article/pii/S2666549221000128>.
- [40] R.T. Cygan, J.-J. Liang, A.G. Kalinichev, Molecular models of hydroxide, oxyhydroxide, and clay phases and the development of a general force field, *J. Phys. Chem. B* 108 (4) (2004) 1255–1266.
- [41] H.J.C. Berendsen, J.R. Grigera, T.P. Straatsma, The missing term in effective pair potentials, *J. Phys. Chem.* 91 (24) (1987) 6269–6271.
- [42] E.J. Maginn, R.A. Messerly, D.J. Carlson, D.R. Roe, J.R. Elliott, Best practices for computing transport properties 1. Self-diffusivity and viscosity from equilibrium molecular dynamics [Article v1.0], *Living J. Comput. Mol. Sci.* 1 (1) (2019), <https://doi.org/10.33011/livecoms.1.1.6324>, 6324–6324, number: 1.
- [43] H. Hatta, M. Taya, Effective thermal conductivity of a misoriented short fiber composite, *J. Appl. Phys.* 58 (7) (1985) 2478–2486.
- [44] M.J.A. Qomi, F.-J. Ulm, R.J.-M. Pellenq, Physical origins of thermal properties of cement paste, *Phys. Rev. Appl.* 3 (6) (2015), 064010.
- [45] P.K. Sarkar, N. Mitra, Thermal conductivity of cement paste: influence of macro-porosity, *Cem. Concr. Res.* 143 (2021), 106385.
- [46] S. Torquato, *Random Heterogeneous Materials: Microstructure and Macroscopic Properties*, Springer Science & Business Media, 2002.

- [47] W.-S. Chiang, E. Fratini, P. Baglioni, D. Liu, S.-H. Chen, Microstructure determination of calcium-silicate-hydrate globules by small-angle neutron scattering, *J. Phys. Chem. C* 116 (8) (2012) 5055–5061.
- [48] S. Masoumi, D. Ebrahimi, H. Valipour, M.J.A. Qomi, Nanolayered attributes of calcium-silicate-hydrate gels, *J. Am. Ceram. Soc.* 103 (1) (2020) 541–557.
- [49] M.J. Abdolhosseini Qomi, L. Brochard, T. Honorio, I. Maruyama, M. Vandamme, Advances in atomistic modeling and understanding of drying shrinkage in cementitious materials, *Cem. Concr. Res.* 148 (2021), 106536.
- [50] M. Holz, S.R. Heil, A. Sacco, Temperature-dependent self-diffusion coefficients of water and six selected molecular liquids for calibration in accurate <sup>1</sup>H NMR PFG measurements, *Phys. Chem. Chem. Phys.* 2 (20) (2000) 4740–4742.
- [51] D.R. Lide, G. Baysinger, S. Chemistry, L.I. Berger, R.N. Goldberg, H.V. Kehaian, in: *CRC Handbook of Chemistry and Physics*, 2004, p. 2661.
- [52] P.E. Smith, W.F. van Gunsteren, The viscosity of SPC and SPC/E water at 277 and 300 K, *Chem. Phys. Lett.* 215 (4) (1993) 315–318.
- [53] E. Stora, B. Bary, Q.-C. He, On estimating the effective diffusive properties of hardened cement pastes, *Transp. Porous Media* 73 (3) (2008) 279–295.
- [54] E.D. Gado, A. Fierro, L.D. Arcangelis, A. Coniglio, Slow dynamics in gelation phenomena: from chemical gels to colloidal glasses, *Phys. Rev. E* 69 (5) (2004), 051103.
- [55] T. Honorio, T. Bore, F. Benboudjema, E. Vourc'h, M. Ferhat, Dielectric properties of the pore solution in cement-based materials, *J. Mol. Liq.* 302 (2020), 112548.
- [56] C. Hammond, *Handbook of Chemistry and Physics*, by DR Lide, CRC Press, Boca Raton, FL.
- [57] T. Honorio, T. Lemaire, D.D. Tommaso, S. Naili, Anomalous water and ion dynamics in hydroxyapatite mesopores, *Comput. Mater. Sci.* 156 (2019) 26–34, <https://doi.org/10.1016/j.commatsci.2018.08.060>.
- [58] M.E. Tuckerman, A. Chandra, D. Marx, Structure and dynamics of OH<sup>-</sup> (aq), *Acc. Chem. Res.* 39 (2) (2006) 151–158, <https://doi.org/10.1021/ar040207n>. <https://pubs.acs.org/doi/10.1021/ar040207n>.
- [59] S.T. Roberts, P.B. Petersen, K. Ramasesha, A. Tokmakoff, I.S. Ufimtsev, T. J. Martinez, Observation of a zundel-like transition state during proton transfer in aqueous hydroxide solutions, *Proc. Natl. Acad. Sci.* 106 (36) (2009) 15154–15159, <https://doi.org/10.1073/pnas.0901571106>, <http://www.pnas.org/cgi/doi/10.1073/pnas.0901571106>, <http://www.pnas.org/cgi/doi/10.1073/pnas.0901571106>.
- [60] C.D. Wick, L.X. Dang, Investigating hydroxide anion interfacial activity by classical and multistate empirical valence bond molecular dynamics simulations, publisher: American Chemical Society, *J. Phys. Chem. A* 113 (22) (2009) 6356–6364, <https://doi.org/10.1021/jp900290y>. URL doi:10.1021/jp900290y.
- [61] I.S. Ufimtsev, A.G. Kalinichev, T.J. Martinez, R.J. Kirkpatrick, A multistate empirical valence bond model for solvation and transport simulations of OH<sup>-</sup> in aqueous solutions, URL, *Phys. Chem. Chem. Phys.* 11 (41) (2009) 9420–9430, <https://doi.org/10.1039/B907859B>, <https://pubs.rsc.org/en/content/articlelanding/2009/cp/b907859b>.
- [62] D. Dong, W. Zhang, A.C.T. van Duin, D. Bedrov, Grotthuss versus vehicular transport of hydroxide in anion-exchange membranes: insight from combined reactive and nonreactive molecular simulations, publisher: American Chemical Society, *J. Phys. Chem. Lett.* 9 (4) (2018) 825–829, <https://doi.org/10.1021/acs.jpcclett.8b00004>. URL doi:10.1021/acs.jpcclett.8b00004.
- [63] H. Li, E. Fratini, W.-S. Chiang, P. Baglioni, E. Mamontov, S.-H. Chen, Dynamic behavior of hydration water in calcium-silicate-hydrate gel: a quasielastic neutron scattering spectroscopy investigation, *Phys. Rev. E* 86 (6) (2012), 061505.
- [64] E. Fratini, A. Faraone, F. Ridi, S.-H. Chen, P. Baglioni, Hydration water dynamics in tricalcium silicate pastes by time-resolved incoherent elastic neutron scattering, *J. Phys. Chem. C* 7 (2013).
- [65] T. Honorio, H. Carasek, O. Cascudo, Electrical properties of cement-based materials: multiscale modeling and quantification of the variability, *Constr. Build. Mater.* 245 (2020), 118461.